OXFORD

Human Molecular Genetics, 2017, Vol. 26, No. 23 4541–4555

doi: 10.1093/hmg/ddx333
Advance Access Publication Date: 30 August 2017
Original Article

ORIGINAL ARTICLE

In vitro characterization of mitochondrial function and structure in rat and human cells with a deficiency of the NADH: ubiquinone oxidoreductase Ndufc2 subunit

Salvatore Raffa[1,4], Cristina Scrofani[1], Sabatino Valente[1], Andrea Micaloni[1], Maurizio Forte[2], Franca Bianchi[2], Roberta Coluccia[2], Aron M. Geurts[3], Sebastiano Sciarretta[2,5], Massimo Volpe[1,2], Maria Rosaria Torrisi[1,4] and Speranza Rubattu[1,2,*]

[1]Department of Clinical and Molecular Medicine, School of Medicine and Psychology, Sapienza University of Rome, Rome, Italy, [2]I.R.C.C.S. Neuromed, Pozzilli (Isernia), Italy, [3]Department of Physiology and Human and Molecular Genetics Center, Medical College of Wisconsin, Milwaukee, WI, USA, [4]Cellular Diagnostics Unit, Azienda Sant'Andrea University Hospital, Rome, Italy and [5]Department of Medical-Surgical Sciences and Biotechnologies, Sapienza University of Rome, Latina, Italy

*To whom correspondence should be addressed at: Department of Clinical and Molecular Medicine, School of Medicine and Psychology, Sapienza University, Rome, Italy and IRCCS Neuromed, Pozzilli, Italy. Tel: 0039 0633775979; Fax: 0039 0633775061; Email: rubattu.speranza@neuromed.it

Abstract

Ndufc2, a subunit of the NADH: ubiquinone oxidoreductase, plays a key role in the assembly and activity of complex I within the mitochondrial OXPHOS chain. Its deficiency has been shown to be involved in diabetes, cancer and stroke. To improve our knowledge on the mechanisms underlying the increased disease risk due to Ndufc2 reduction, we performed the present *in vitro* study aimed at the fine characterization of the derangements in mitochondrial structure and function consequent to Ndufc2 deficiency. We found that both fibroblasts obtained from skin of heterozygous *Ndufc2* knock-out rat model showed marked mitochondrial dysfunction and PBMC obtained from subjects homozygous for the TT genotype of the rs11237379/NDUFC2 variant, previously shown to associate with reduced gene expression, demonstrated increased generation of reactive oxygen species and mitochondrial damage. The latter was associated with increased oxidative stress and significant ultrastructural impairment of mitochondrial morphology with a loss of internal cristae. In both models the exposure to stress stimuli, such as high-NaCl concentration or LPS, exacerbated the mitochondrial damage and dysfunction. Resveratrol significantly counteracted the ROS generation. These findings provide additional insights on the role of an altered pattern of mitochondrial structure–function as a cause of human diseases. In particular, they contribute to underscore a potential genetic risk factor for cardiovascular diseases, including stroke.

Received: June 26, 2017. **Revised:** August 21, 2017. **Accepted:** August 22, 2017

© The Author 2017. Published by Oxford University Press.
This is an Open Access article distributed under the terms of the Creative Commons Attribution Non-Commercial License (http://creativecommons.org/licenses/by-nc/4.0/), which permits non-commercial re-use, distribution, and reproduction in any medium, provided the original work is properly cited. For commercial re-use, please contact journals.permissions@oup.com

Introduction

The oxidative phosphorylation chain, located within the inner mitochondrial membrane, is a fundamental component for life of all organisms (1). Among the five OXPHOS complexes, the complex I (CI), known as NADH: ubiquinone oxidoreductase, exerts important functions since it processes NADH to produce electrons and to reduce molecular oxygen to form H_2O. CI contributes about 40% of the proton motive force that drives ATP synthesis by ATP synthase, and it is a major source of mitochondrial anion superoxide production (2). A dysfunctional CI results in increased mitochondrial reactive oxygen species (ROS) accumulation and deleterious cellular effects that may represent the basis of several pathological conditions, including cardiovascular diseases (2,3). Of interest, NDUFC2 is one of the 45 subunits composing CI and is encoded by nuclear DNA. Recently, we and others discovered a key role of NDUFC2 in CI assembly and activity by showing that its lack does not allow a regular OXPHOS function (4,5). In particular, we demonstrated that NDUFC2 inhibition by high-salt diet promotes cerebrovascular accidents in an animal model of spontaneous hypertension and stroke (5); that a stroke-resistant animal model developed stroke when it carried *Ndufc2* deletion in a heterozygous configuration (5); and finally that human subjects carrying a *NDUFC2* variant associated with reduced protein expression level had a significant increased risk of juvenile ischemic stroke (5). A dysfunctional NDUFC2 gene is also involved in the pathogenesis of diabetes and of few types of cancer (4,6–8). Notably, NDUFC2 pharmacological stimulation promises to be helpful in the treatment of myocardial infarction (9). Thus, the critical functions played by this CI subunit in health and disease require a further investigation in order to better understand the pathogenesis of the clinical conditions derived from a defective CI activity.

We previously reported the molecular effects of NDUFC2 suppression in silenced vascular murine cells (5). In the present study, we performed a detailed investigation of the deleterious consequences of NDUFC2 deficiency on mitochondrial function and structure in primary mesenchymal cells obtained from the previously reported knock-out rat model (5) and in PBMCs obtained from apparently healthy human subjects carrying the gene variant associated with decreased protein expression (5). By performing this approach we aimed to fully characterize a novel genetic disease risk factor.

Results

The *Ndufc2* deficiency is related to mitochondrial dysfunction and ultrastructural damage in fibroblasts from the heterozygous knock-out rat model

We previously demonstrated that CI assembly/activity and mitochondrial membrane potential were significantly reduced in brain tissue from a rat model heterozygous for an engineered *Ndufc2* deletion, in particular upon a high-salt Japanese-style stroke permissive diet (JD) (5).

In order to study the function and structure of mitochondria in cells deficient for the NDUFC2 subunit of CI, we isolated and propagated in culture primary skin fibroblasts from heterozygous SHRSR_KO *Ndufc2* and control SHRSR_WT rats (see Materials and methods and Supplementary materials) and $\Delta\psi m$ and intracellular levels of ROS in either unstimulated or high-NaCl treated primary cultures were compared. Under basal experimental conditions the amount of actively respiring mitochondria (MT-Red staining; Fig. 1A and B), the $\Delta\psi m$ values (TMRM staining; Fig. 2C), the mitochondrial depolarization index and the percentage of cells with a low mitochondrial membrane potential (JC-1 staining; Fig. 1E and F) were similar among cultures. Conversely, SHRSR_KO *Ndufc2* fibroblasts showed a time-dependent reduction of $\Delta\psi m$ and mitochondrial depolarization index which reached the lowest peak at 72 hours in response to high-NaCl medium compared with SHRSR_WT fibroblasts ($P < 0.05$ for TMRM and $P < 0.01$ for JC-1 staining versus basal levels; Fig. 1D and G, respectively).

To assess whether the mitochondrial dysfunction observed in the SHRSR_KO *Ndufc2* fibroblasts could be related to the generation of increased oxidative stress, we evaluated the intracellular ROS levels by cytofluorimetric analysis. At baseline and during the time-course exposure to high-NaCl medium, the SHRSR_KO *Ndufc2* cells generated greater amounts of intracellular and mitochondrial ROS than those produced from the SHRSR_WT fibroblasts (Fig. 2A and C; $P < 0.05$ at each experimental time points); moreover, no significant increase of ROS levels was documented in either fibroblast culture during high-salt exposure (Fig. 2B and D; test for linear trend: $P = \text{NS}$ for SHRSR_WT and KO *Ndufc2* fibroblasts).

In order to investigate whether the impairment of NADH: ubiquinone oxidoreductase related to Ndufc2 deficiency could be also responsible of structural alterations in mitochondrial membrane system in our cellular model, we considered two parameters of ultrastructural degeneration: i) the percentage of mitochondrial area carrying intact cristae; and ii) the loss of IMM assessed as the IMM/OMM index (10). We quantified a grading of the morphological damage categorized as i) slight; ii) moderate; and iii) severe, according to the three levels (called Mt-G1–3).

At baseline, the amount of mitochondria with normal ultrastructure or with slight damage (Mt-G1) was similar among cultures (Fig. 3A,C and F); on the other hand, the Mt-G2 category was observed in 35% and 15% (ratio 2.3) of the mitochondrial population of the SHRSR_KO *Ndufc2* and SHRSR_WT fibroblasts, respectively. The severe damage (Mt-G3) category was observed only in the mitochondrial population of SHRSR_KO *Ndufc2* cells (2%) and the overall damage (Mt-G1 + 2 + 3) was observed in 70% of SHRSR_KO *Ndufc2* compared with 45% of SHRSR_WT fibroblasts, with a total ratio of 1.55 ($P < 0.05$; Fig. 3A). After 72 hours of high-NaCl exposure, the SHRSR_WT fibroblasts showed no significant changes of mitochondrial damage score (Fig. 3A,D and E); in contrast, the high-NaCl exposure further enhanced the mitochondrial damage in SHRSR_KO-*Ndufc* cells (Fig. 3G and H), with an overall damage of 85% ($P < 0.05$ vs unstimulated SHRSR_KO *Ndufc2* cells; Fig. 3A).

Importantly, these data were corroborated by the IMM/OMM index associated with convolution loss of inner mitochondrial membrane. The latter was characterized by the values of 1.72 ± 0.01 and of 2.02 ± 0.02 in the SHRSR_KO *Ndufc2* cells exposed or not to high-NaCl, respectively ($P < 0.05$; Fig. 3B). In contrast, SHRSR_WT fibroblasts showed higher IMM/OMM index values, with minimal and no significant changes after high-NaCl exposure, which reflected the preservation of the integrity of mitochondria ultrastructure even after stimulation (Fig. 3D and E).

To assess whether the ROS production could be directly involved in the onset of mitochondrial dysfunction and mitochondrial morphology impairment, the SHRSR_KO *Ndufc2* and SHRSR_WT cells were pretreated with resveratrol 50 μM for 12 hours before the salt stimulation, a natural molecule with anti-inflammatory and antioxidant action able to exert strong inhibitory effects on ROS generation (11). In our experimental

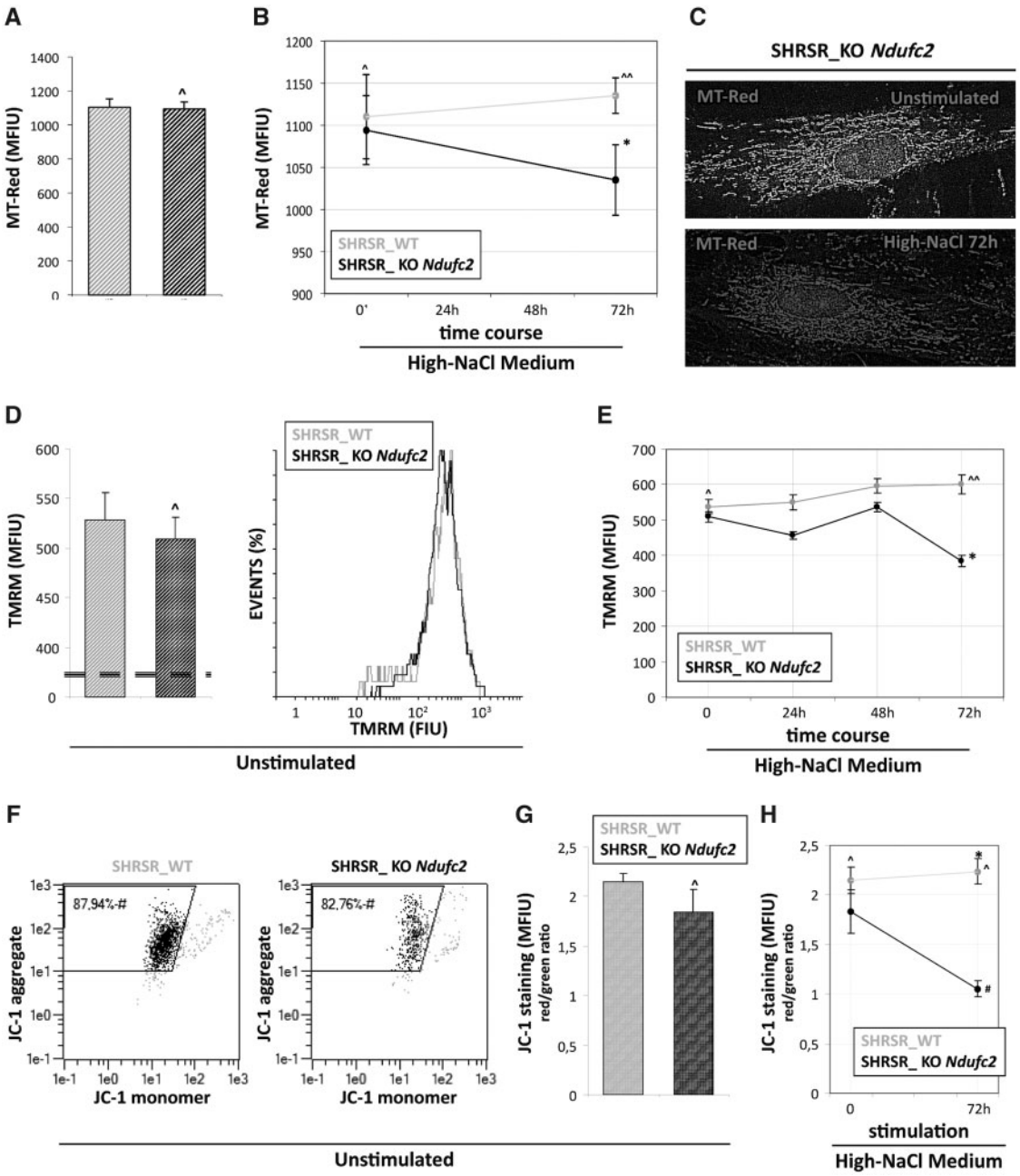

Figure 1. Evaluation of mitochondrial dysfunction in fibroblasts from SHRSR_KO-*Ndufc2*. **(A,B)** Quantitative fluorescence analysis of MT-Red^{TM} staining under basal experimental condition (A) and after exposure to high-NaCl medium (B). The amount of active mitochondria was similar among unstimulated cultures (Student *t* test: ^P = NS versus SHRSR_WT) whereas after salt stimulus the SHRSR_KO-*Ndufc2* fibroblasts showed a reduction of MT-Red staining respect to SHRSR_WT (Student *t* test: *P < 0.05). **(C)** The elaboration of MT-Red levels by a rainbow pseudo-color scale shows a brown-red staining in SHRSR_KO-*Ndufc2* salt stimulated cells, reflecting the lowest intensity values of MT-Red. **(D–E)** TMRM cytofluorimetric assay for mitochondrial membrane potential ($\Delta\psi$m). Under basal experimental condition (D) the $\Delta\psi$m values were similar among unstimulated cultures (Student *t* test:^P = NS versus SHRSR_WT). In time-course experiment under exposure to high-NaCl medium the fibroblast cultures displayed a different response to salt stimulus (E); respect to SHRSR_WT fibroblasts. The SHRSR_KO-*Ndufc2* fibroblasts showed a time-dependent reduction of $\Delta\psi$m with a lowest peak at 72 hours (Student *t* test: ^P = NS versus SHRSR_WT; one-way ANOVA with test for linear trend: ^P = NS; *P < 0.05). **(F–H)** JC-1 cytofluorimeric assay. Under basal conditions the percentage of cells with a low mitochondrial membrane potential (F) and the mitochondrial depolarization index (G) were similar among cultures (Student *t* test: ^P = NS). After high-NaCl stimulus (H), the SHRSR_KO-*Ndufc2* fibroblasts showed a significant reduction of mitochondrial depolarization index respect to SHRSR_WT fibroblasts (one-way ANOVA with test for linear trend: *P < 0.05).

setting, resveratrol dampened the mitochondrial depolarization (Fig. 4B), the mitochondrial oxidative stress (Fig. 4C) and the mitochondrial morphological damage (Fig. 4D–L) observed after high-NaCl exposure. As expected, no significant changes were observed in SHRSR_WT cells (data not shown).

Altogether, our data indicate that *Ndufc2* deficiency determines the appearance of mitochondrial dysfunction with increased generation of intracellular ROS. As expected, these conditions were also associated with the onset of strong alteration of mitochondrial morphology, as a loss of internal cristae,

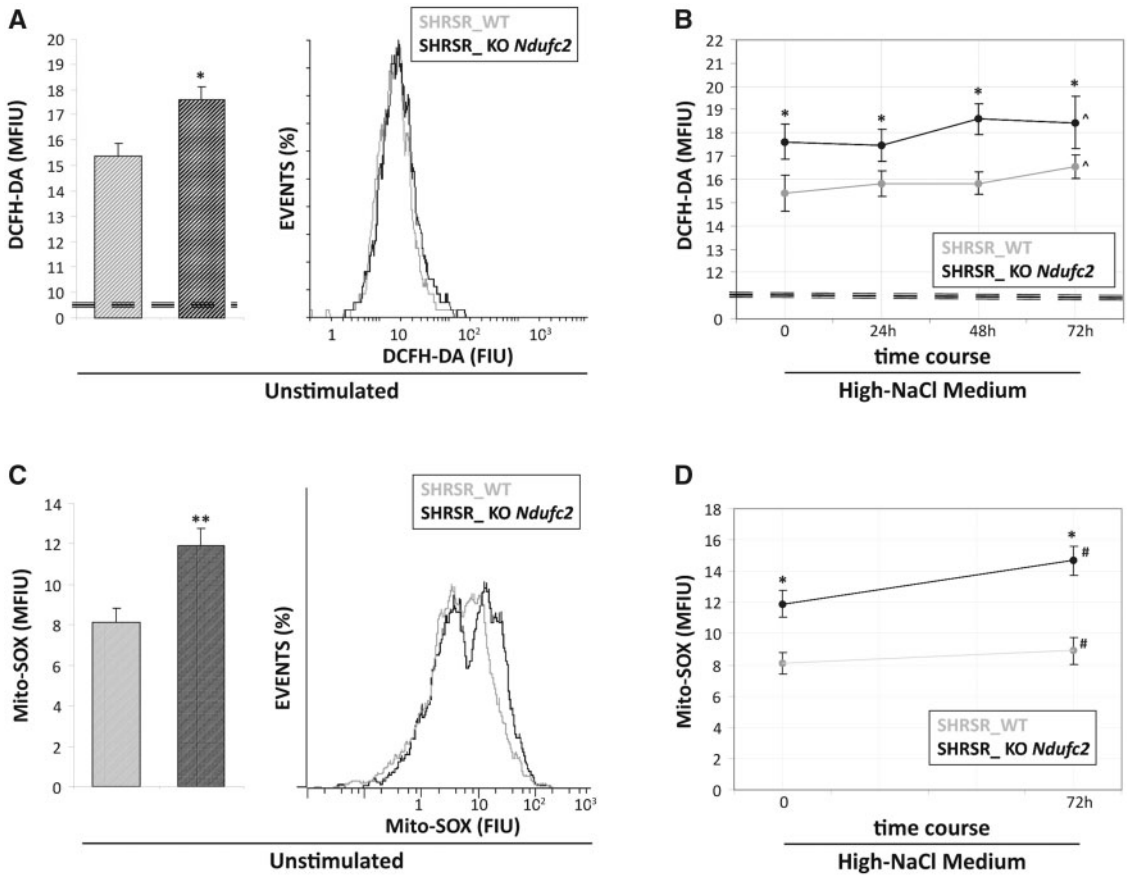

Figure 2. Reactive oxygen species detection in fibroblasts from SHRSR_KO-*Ndufc2*. Both at baseline and during all points of the time-course experiment, the SHRSR_KO-*Ndufc2* cells generated greater amounts of cytoplasmic (**A**) and mitochondrial ROS (**C**) compared with those produced from the SHRSR_WT fibroblasts (Student *t* test: $^{*}P < 0.05$ for all experimental points). No significant increases of ROS levels (**B** and **D**) were documented in both fibroblast cultures during high-salt exposure (one-way ANOVA with test for linear trend: $^{\wedge}$ and $^{\#}P = \text{NS}$).

and were also exacerbated by exposure to high-NaCl concentration. The crucial role exerted by oxidative stress on the dysfunction and ultrastructural impairment of the mitochondria was confirmed by the counteracting effects of resveratrol.

Oxidative stress and mitochondrial damage characterize PBMCs from subjects carrying a gene variant associated with decreased NDUFC2 expression

To test whether the results obtained in heterozygous *Ndufc2* knockout rat model occur also in humans, we aimed to study the PBMCs obtained from apparently healthy subjects carrying the T allele at rs11237379 associated with decreased NDUFC2 expression (5). The T and C rs11237379 alleles are present in the general population at 66% and 34%, respectively according to Phase 3 of the 1000 Genomes Project. (12). In the present study, we confirmed that NDUFC2 expression was 1.58 ± 0.3 in CC, 0.4 0.08 in TC, 0.27 ± 0.07 in TT subjects (Supplementary Material, Fig. S2).

In order to analyse the mitochondrial function at basal condition, we assessed levels of $\Delta\psi$m and of intracellular and mitochondrial ROS concentration in the PBMCs obtained from homozygous (TT) and heterozygous (TC) subjects for the rs11237379 allele with respect to PBMCs from subjects homozygous for the minor allele (CC). The flow cytometric analysis of mitochondrial membrane potential by TMRM and JC-1 staining showed no significant differences between the groups of PBMCs (Fig. 5A and C), although the ROS levels tended to be higher in T allele carriers (Fig. 6A and C).

To unmask possible differences between groups of PBMCs, we re-analysed the $\Delta\psi$m levels after stimulation for 48 hours with high-NaCl medium and with a standardized inflammatory stimulus (1 μg/ml Lipopolysaccharide S). As expected, and similarly to what observed in primary rat fibroblasts, the high-NaCl stimulus induced changes of $\Delta\psi$m significantly higher in PBMCs from subjects carrying both TT and TC genotypes ($\Delta\psi$m fold changes: 0.8 and 0.81 respectively vs unstimulated cells) with respect to PBMCs from CC carriers ($\Delta\psi$m 0.93 fold changes vs unstimulated cells; $P < 0.05$; Fig. 5B). The stimulation with LPS alone produced similar results. This data were corroborated by JC-1 staining changes reflecting a significant mitochondrial depolarization in PBMCs from TT compared with CC subjects (0.93 vs 0.85 fold changes vs unstimulated cells; $P < 0.05$; Fig. 5D). In addition, cytoplasmic and mitochondrial ROS levels were significantly higher in PBMCs from TT subjects to NaCl and LPS compared with PBMCs from both heterozygous TC and CC carriers (Fig. 6B and D).

Based on the above-described functional data, we wanted to quantify the morphological alterations also in mitochondria from human PBMCs samples treated or not as above. At baseline, the distribution of Mt-G categories and the burden of

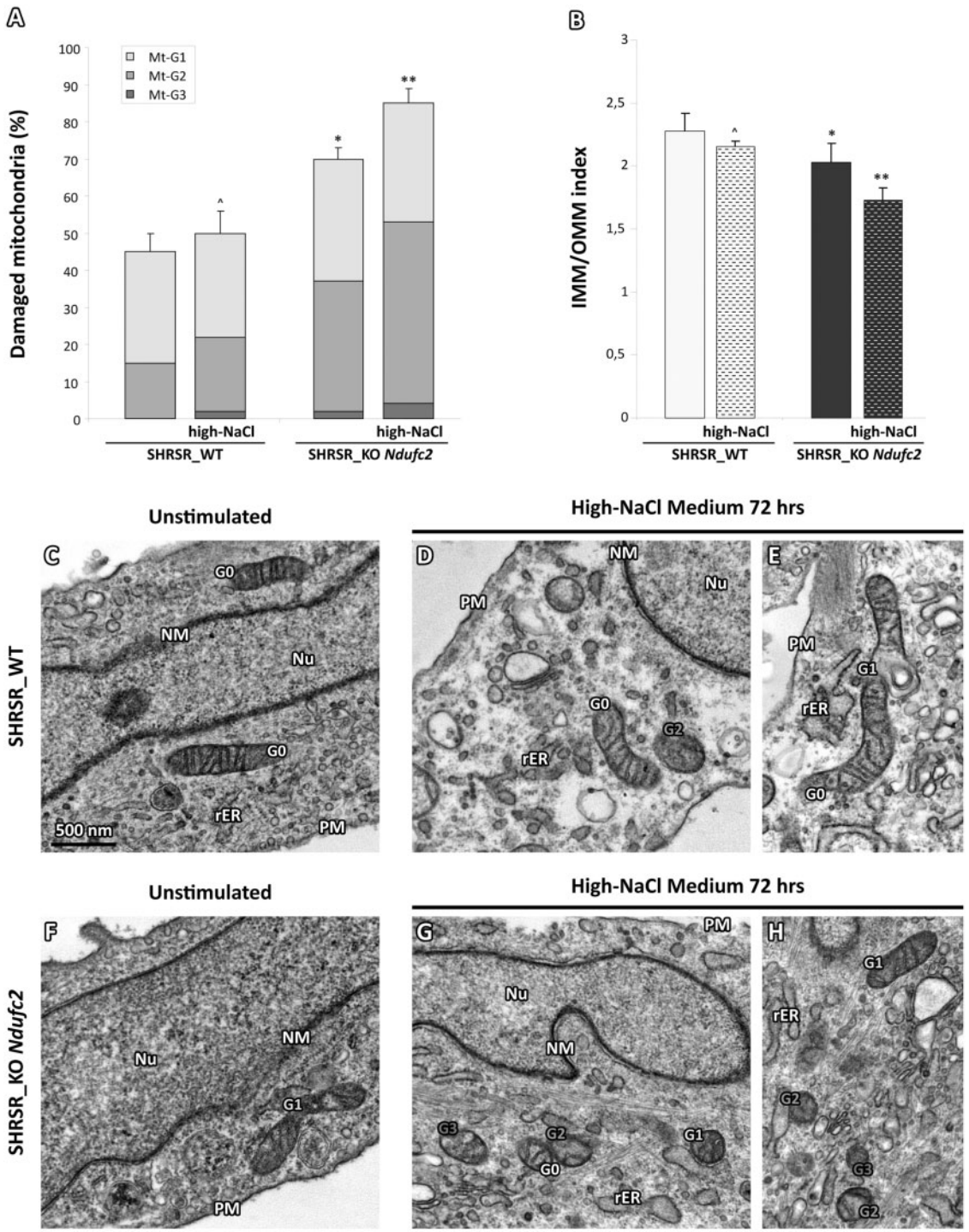

Figure 3. Evaluation of ultrastructural damage in mitochondria from SHRSR_KO *Ndufc2* fibroblasts. (**A,B**) Graphical representation of the ultrastructural damage in SHRSR_WT and _KO-*Ndufc2* fibroblasts; the injury was quantified on the basis of the percentage of mitochondrial area displaying intact cristae (A) and convolution degree (B). At baseline, a severe damage (Mt-G3) was observed only in the mitochondria of SHRSR_KO-*Ndufc2*. The overall damage (Mt-G1 + 2+3) and the loss of inner cristae (IMM/OMM index) were higher in KO compared with WT fibroblasts (Kruskal-Wallis test in (A and B): $^{*}P < 0.05$). Respect to baseline conditions, the salt stimulus enhanced the mitochondrial damage in KO (Kruskal-Wallis test in (A and B): $^{**}P < 0.05$) but not in WT fibroblasts (Kruskal-Wallis test in (A and B): $^{\wedge}P = NS$). (**C–H**) Representative micrographs of mitochondria in unstimulated or high-NaCl exposed fibroblasts. After salt stimulus, the mitochondria from KO fibroblasts showed a marked loss of cristae (G and H); in contrast, WT fibroblasts (D and E) displayed organelles with normal ultrastructural findings or only with a minor damage. (TEM micrographs, uranyl acetate/lead citrate; Legend: Nu, nucleus; NM, nuclear membrane, PM, plasma membrane; rER, rough endoplasmic reticulum; Gx: grade of mitochondrial damage).

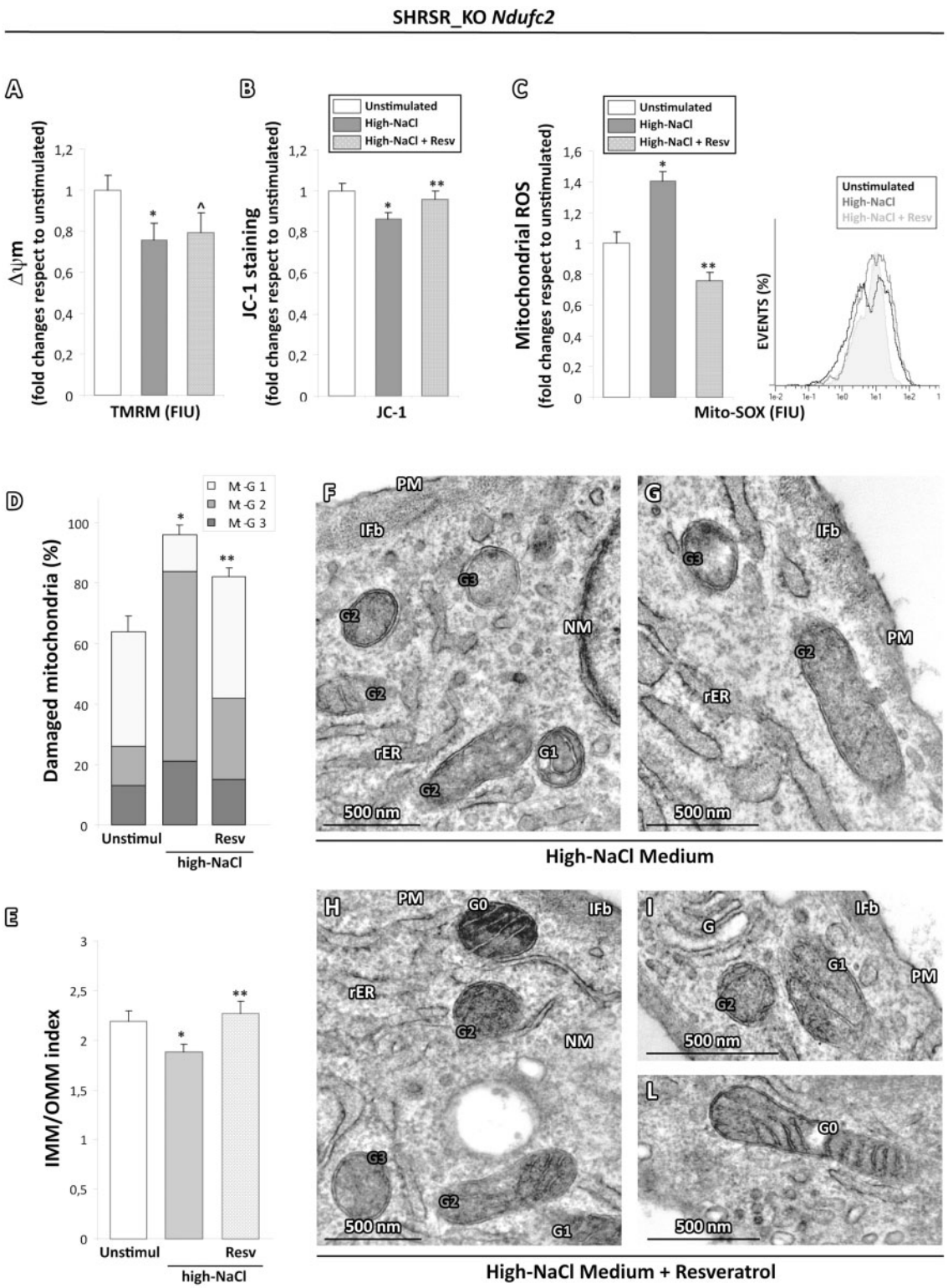

Figure 4. Effects of ROS scavenging on the high-salt dependent functional and ultrastructural impairment in mitochondria from SHRSR_KO Ndufc2 fibroblasts. (**A,B**) TMRM (A) and JC-1 (B) cytofluorimetric assay for mitochondrial membrane potential evaluation ($\Delta\psi m$). The pretreatment with resveratrol dampened the mitochondrial depolarization induced by high-salt stimulation (Student *t* test: $^{*}P < 0.05$ vs unstimulated SHRSR_KO *Ndufc2*; $\hat{}P < 0.05$ vs unstimulated SHRSR_KO *Ndufc2* and $P = NS$ vs salt stimulated SHRSR_KO *Ndufc2*; $\hat{}P < 0.05$ vs unstimulated and salt stimulated SHRSR_KO *Ndufc2*). (**C**) Mito-SOX cytofluorimetric assay for mitochondrial ROS generation. The resveratrol counteracted the oxidative stress due to high-salt stimulation (Student *t* test: $^{*}P < 0.05$ versus unstimulated SHRSR_KO *Ndufc2*; $^{**}P < 0.01$ vs salt stimulated SHRSR_KO *Ndufc2*; see the pale grey area versus the grey line in the histogram) (**D,E**) Graphical representation of resveratrol treatment effects on the ultrastructural damage due to salt stimulation in SHRSR_KO *Ndufc2* fibroblasts. The overall damage (Mt-G1 + 2+3) and the loss of inner cristae (IMM/OMM index) were lower in SHRSR_KO *Ndufc2* fibroblasts treated with resveratrol compared with stimulated SHRSR_KO *Ndufc2* (Kruskal-Wallis test in (D and E): $^{**}P < 0.05$ vs salt stimulated SHRSR_KO *Ndufc2*). (**F–I,L**) Representative micrographs of mitochondria in high-NaCl exposed SHRSR_KO *Ndufc2* fibroblasts, preatreated or not with resveratrol. After salt stimulus, the mitochondria from KO *Ndufc2* fibroblasts showed a marked loss of cristae (F and G); in contrast, KO *Ndufc2* fibroblasts pretreated with resveratrol (H, I and L) displayed organelles with a minor grade of damage. (TEM micrographs, uranyl acetate/lead citrate; Legend: Nu, nucleus; NM, nuclear membrane, PM, plasma membrane; rER, rough endoplasmic reticulum; IFb, intermediate filament bundles; Gx: grade of mitochondrial damage).

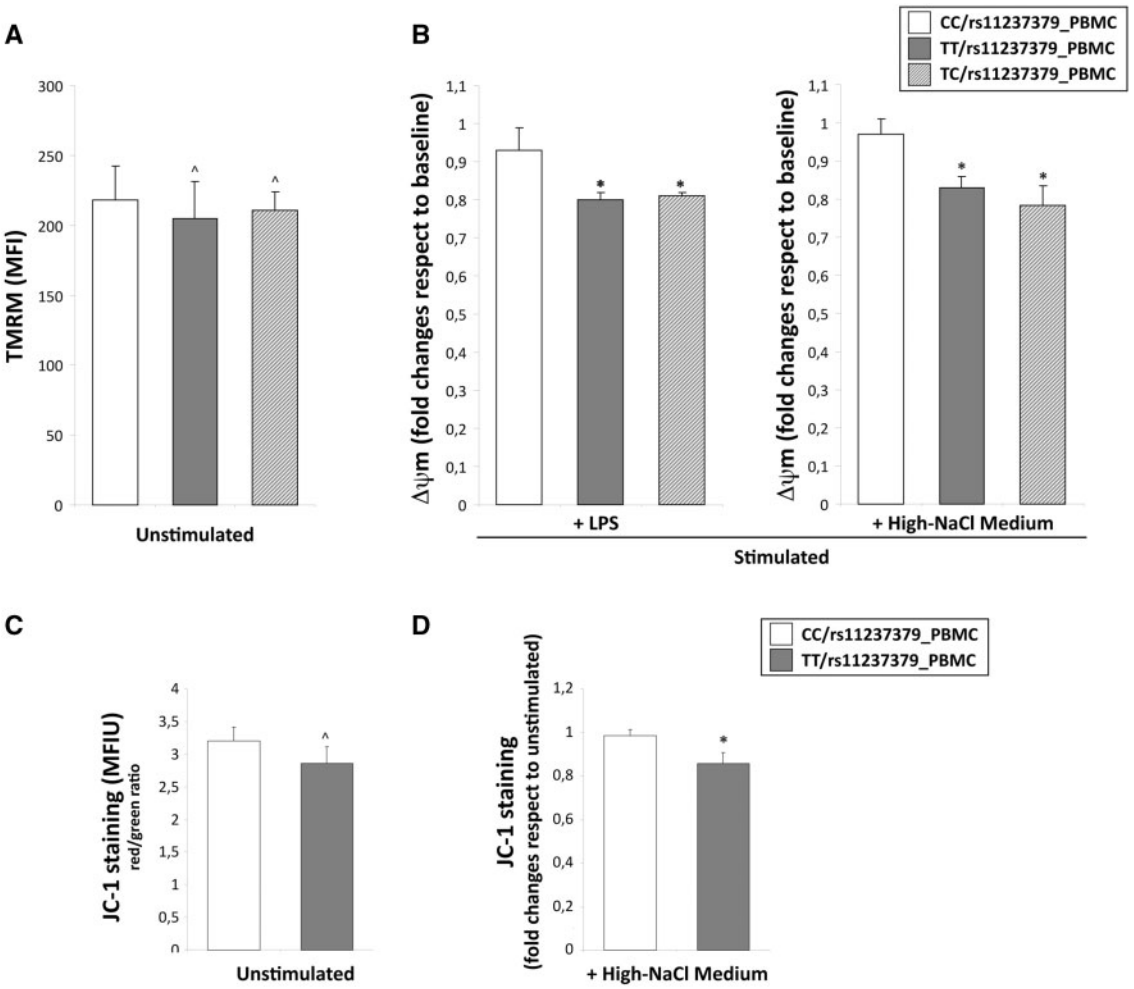

Figure 5. Evaluation of mitochondrial depolarization in human PBMCs obtained from carriers of rs11237379 gene variant associated with decreased NDUFC2 expression. **(A–D)** Cytofluorimetric assay for mitochondrial membrane potential ($\Delta\psi m$) at baseline and under stimulation with LPS or high-salt medium. The $\Delta\psi m$ values among the unstimulated PBMCs obtained from homozygous (TT) and heterozygous (TC) carriers for the rs11237379 and PBMCs from carriers of wild-type genotype (CC) were similar (A and C; one-way ANOVA with Dunnett's test: $\hat{}P = NS$ versus PBMCs from CC genotype). After high-salt or LPS stimulation only PBMCs from TT and TC genotypes showed significant $\Delta\psi m$ reductions with respect to baseline levels (B and D; one-way ANOVA with Dunnett's test: $^*P < 0.05$ versus PBMCs from healthy controls).

overall damage were similar among TC and CC subject PBMCs (55% and 55.5%; $P = NS$; Figs 7A, 8A and I); in contrast, PBMCs from TT subjects showed an overall damage significantly higher with respect to PBMCs from TC and CC subjects (71%; $P < 0.01$; Figs 7A and 8D). The high-NaCl exposure produced a strong increase in the percentages of all Mt-G categories with an overall damage of 86% in the PBMCs from TT subjects (Fig. 8K). Of note, PBMCs from TC and CC carriers showed a slight and not significant increase of mitochondrial overall damage (63% and 62%, respectively), as compared with baseline conditions in the absence of stimulus (Fig. 7A).

These findings were corroborated by the IMM/OMM index analysis, which was characterized by the values of 1.94 ± 0.05 and 1.6 ± 0.05 for PBMCs of TT subjects exposed or not to high-NaCl medium ($P < 0.05$; Fig. 7B). Consistently with what observed in the Mt-grading assessment, a slight no significant reduction of the IMM/OMM values was observed in PMBCs from TC and CC subjects after exposure to high-NaCl (Fig. 8C and K). Finally, the standardized stimulation with LPS produced effects similar to those observed with high-NaCl stimulation in all PBMCs cultures (Fig. 8B, E, F and J).

To evaluate whether, also in human PBMCs, the treatment with ROS scavengers could affect the alterations of mitochondrial parameters, the PBMCs from TT and CC subjects were pretreated before the salt stimulation with resveratrol. As expected, the PBMCs from CC subjects did not show any change of all mitochondrial parameters (data not shown). In contrast, similarly to *in vitro* rat model, resveratrol was able to exert a strong scavenging effect on ROS generation (Fig. 9B), to counteract the mitochondrial membrane depolarization (Fig. 9A) and the overall burden of ultrastructural damage induced by the high-NaCl stimulation (Fig. 9C–H).

Taken together, our results clearly indicated that a decreased NDUFC2 expression related to T/C rs11237379 gene variant determined a status of mitochondrial dysfunction and of increased oxidative stress which was associated with ultrastructural impairment of mitochondrial morphology, similarly to what we observed in primary fibroblasts from the *Ndufc2* heterozygous knock-out rat model. In addition, in both models, the mitochondrial damage was exacerbated by high-NaCl exposure and counteracted by the scavenging of intracellular ROS.

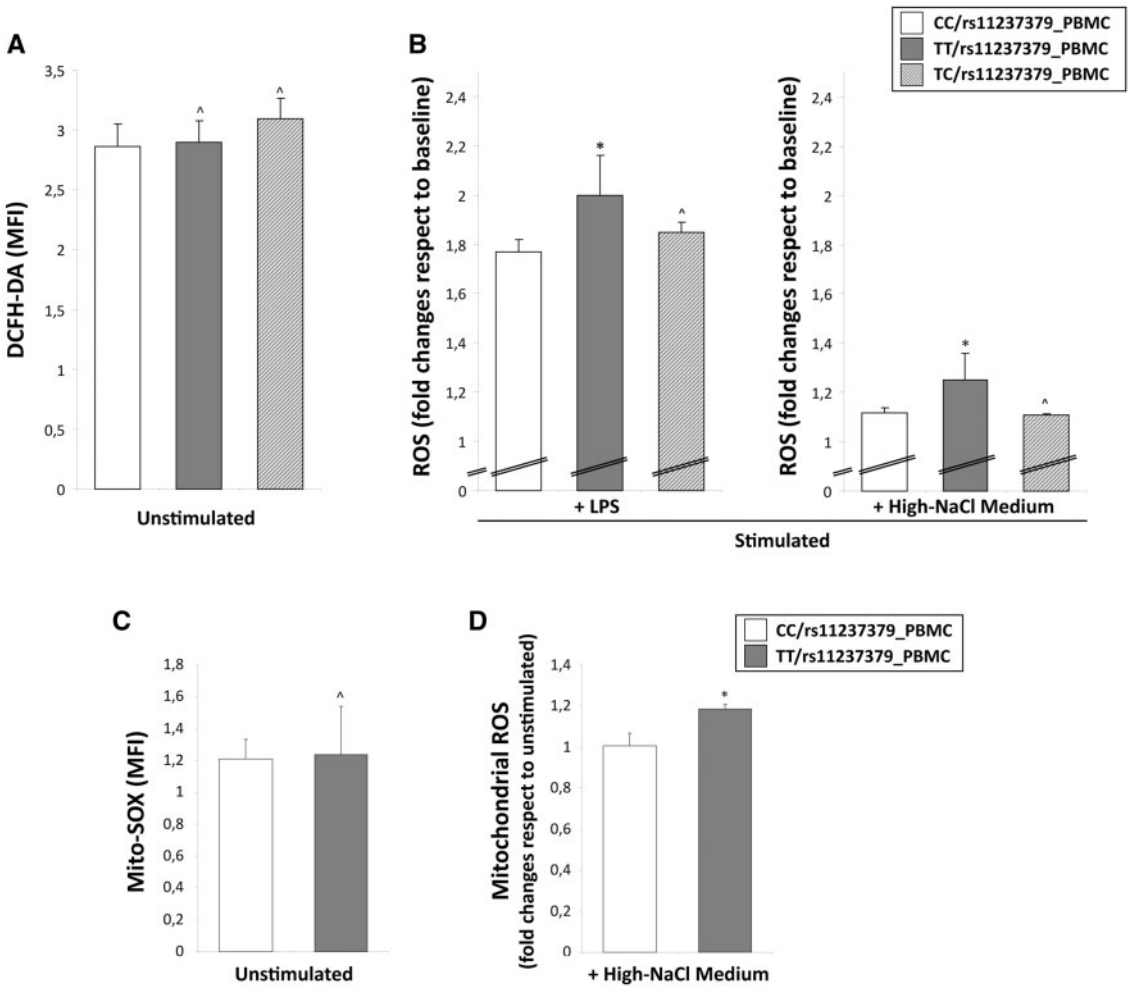

Figure 6. Reactive oxygen species detection in human PBMCs obtained from carriers of rs11237379 gene variant associated with decreased NDUFC2 expression. Cytofluorimetric assay of intracellular and mitochondrial ROS generation in unstimulated or stimulated PBMCs with either LPS or high-salt medium. At baseline, the intracellular (**A**) and mitochondrial (**C**) ROS levels were comparable between the all groups of PBMCs (one-way ANOVA with Dunnett's test: ^P = NS versus PBMCs from healthy controls). The stimulation for 48 hours with high-NaCl or LPS induced a significant increase of ROS levels only in PBMCs from TT carriers (**B** and **D**; one-way ANOVA with Dunnett's test: *$P < 0.05$ and ^P=NS versus PBMCs from CC carriers).

Discussion

According to the classic paradigm of mitochondrial structure–function postulated by Hackenbrock (13,14), any alteration of mitochondrial bioenergetic can determine in a highly dynamic way structural changes of mitochondrial architecture compromising, in turn, the biochemical activities associated with its internal membrane and matrix. Several experimental contributions have subsequently demonstrated that alterations in mitochondrial metabolism can exert an impact on the mitochondrial architecture (15,16). In fact, many of the OXPHOS defects are responsible for an impairment of mitochondrial ultrastructure, with alteration of cristae and reduced convolution of inner mitochondrial membrane that are paralleled by an increased oxidative stress and a decreased cellular ATP content.

The mitochondrial protein Ndufc2 is a key component of NADH dehydrogenase since it plays crucial functions in the inner mitochondrial membrane to allow the normal CI assembly and activity (4,5). The CI is the largest complex of the mitochondrial OXPHOS system and is considered the major ROS-generating site within the mitochondria. Mutations in nuclear-encoded subunits of CI are associated with disorders affecting brain, skeletal muscle, and the heart (17). In particular, the CI dysfunction is able to increase the mitochondrial ROS production and it leads to aberrant mitochondrial morphology (18).

The function of the Ndufc2 subunit is starting to be understood (2) and its pathological relevance has been so far documented in humans with regard to type-2 diabetes mellitus, breast and colorectal cancer (4,6–8). In this scenario, we previously demonstrated (5) that *Ndufc2* was significantly downregulated by high salt diet in the brain of a rat model of stroke (SHRSP) as compared with its strictly related stroke-resistant control (SHRSR). This evidence was associated with reduced ATP and increased ROS levels, all signs of mitochondrial dysfunction. Moreover, *Ndufc2* silenced vascular smooth muscle cells showed an impairment of CI assembly, reduction of mitochondrial membrane potential and of ATP synthesis, with subsequent generation of increased oxidative stress and reduced cell viability. *In vivo*, a heterozygous *Ndufc2*-KO rat model, obtained from the parental SHRSR strain, showed a deficient CI assembly and, more importantly, once fed with the Japanese-style diet, developed renal damage followed by stroke occurrence, resembling the SHRSP. Likewise, the association of the T allele of

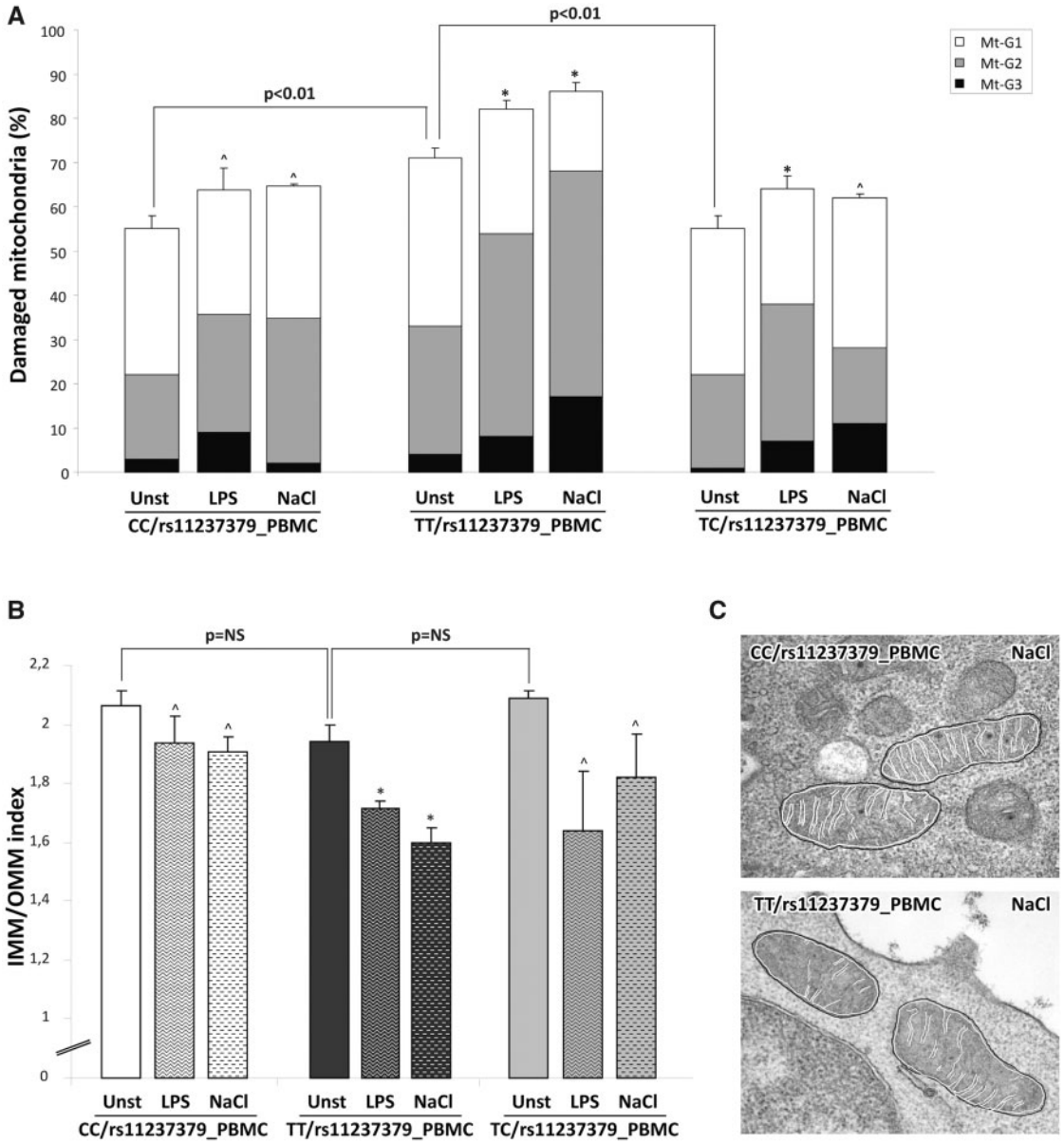

Figure 7. Quantitative analysis of ultrastructural damage in mitochondria from human PBMCs obtained from carriers of rs11237379 gene variant associated with decreased NDUFC2 expression. (**A**) Graphical representation of the ultrastructural Mt-grading of damage. At baseline, the burden of overall damage was higher in PBMCs from subjects carrying homozygous genotype TT respect to PBMCs from TC and CC subjects (Kruskal-Wallis test: $P < 0.01$). The high-NaCl stimulus produced a strong increase of the mitochondrial overall damage only in the PBMCs from TT carriers (one-way ANOVA with Dunnett's test: $^*P < 0.05$ or $\hat{}P = $ NS versus respective unstimulated PBMCs). The standardized stimulation with LPS produced effects similar to those observed after high-salt exposure. (**B**) Graphical representation of the IMM/OMM values. Consistently with Mt-grading analysis, the stimulation with high-salt or LPS induced a significant decrease of IMM/OMM index in the PBMCs from TT carriers (one-way ANOVA with Dunnett's test: $^*P < 0.05$ or $\hat{}$P=NS versus respective unstimulated PBMCs). Representative images are presented in (**C**).

rs11237379 with a significantly reduced NDUFC2 expression and with increased risk of early-onset ischemic stroke (5) supports the hypothesis that reduced NDUFC2 expression could contribute to increased stroke susceptibility also in humans.

In the present study, we attempted to demonstrate whether the NDUFC2 deficiency would be able to determine the ultrastructural damage of mitochondria consistent with the functional impairment of CI and with an increased oxidative stress, as previously shown both *in vitro* and *in vivo*. In particular, we aimed to investigate if a similar morpho-functional impairment would be observed also in PBMCs from healthy carriers with decreased NDUFC2 expression.

For this purpose, we have prepared and characterized primary cultures of fibroblasts from WT and SHRSR_KO *Ndufc2* rats that showed similar morphological, immunophenotypic and ultrastructural findings at baseline condition. In this *in vitro* system, we analysed the mitochondrial response to a stimulation with a high-NaCl concentration medium, in order to reproduce the *in vivo* exposure of rats to a high-salt dietary regimen. As a result, we observed clear signs of mitochondrial suffering, as a $\Delta\psi$m reduction and increased ROS levels only in SHRSR_KO *Ndufc2* fibroblasts. The latter were paralleled by a progressive reduction of mitochondrial area associated with intact cristae, and by a significant reduction of internal

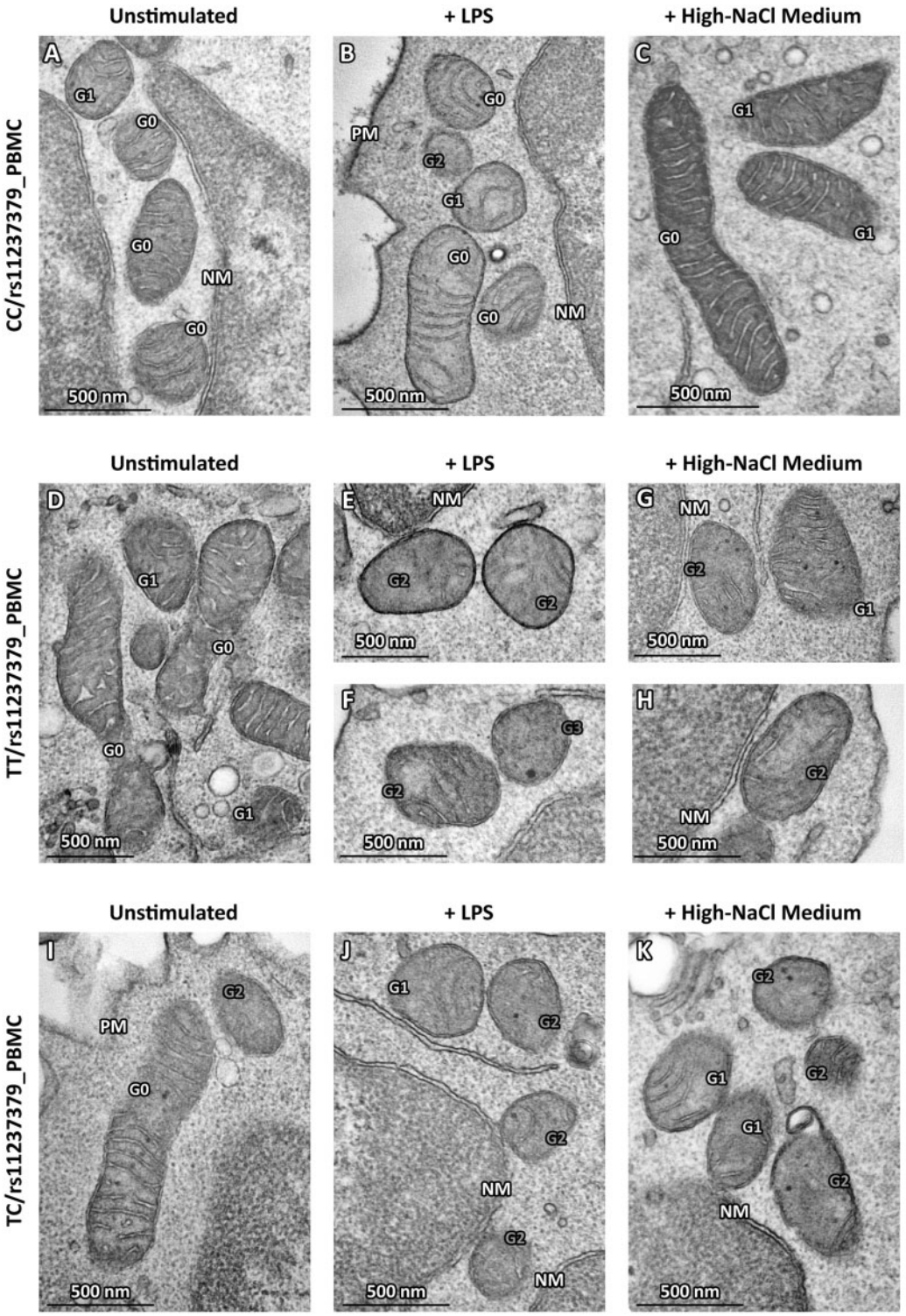

Figure 8. Representative micrographs of ultrastructural damage in mitochondria from human PBMCs obtained from subjects with decreased NDUFC2 expression. The burden of mitochondrial damage after NaCl or LPS stimulation was higher particularly in PBMCs from TT carriers (**E–H**); the mitochondria were characterized by degeneration of convolutions related to lack of the inner membrane and subsequently by reduction of mitochondrial area with intact cristae compared with mitochondria from unstimulated PBMCs (**D**). The mitochondria of PBMCs obtained from healthy subjects showed mitochondria with normal morphology (**A**) or only with slight damage after stimulation (**B,C**). The mitochondria of PBMCs from carriers of heterozygous genotype CT displayed a pattern of intermediate damage (**I**), particularly after stimulation (**J,K**). (TEM micrographs, uranyl acetate/lead citrate; Legend: NM, nuclear membrane, PM, plasma membrane; Gx: grade of mitochondrial damage).

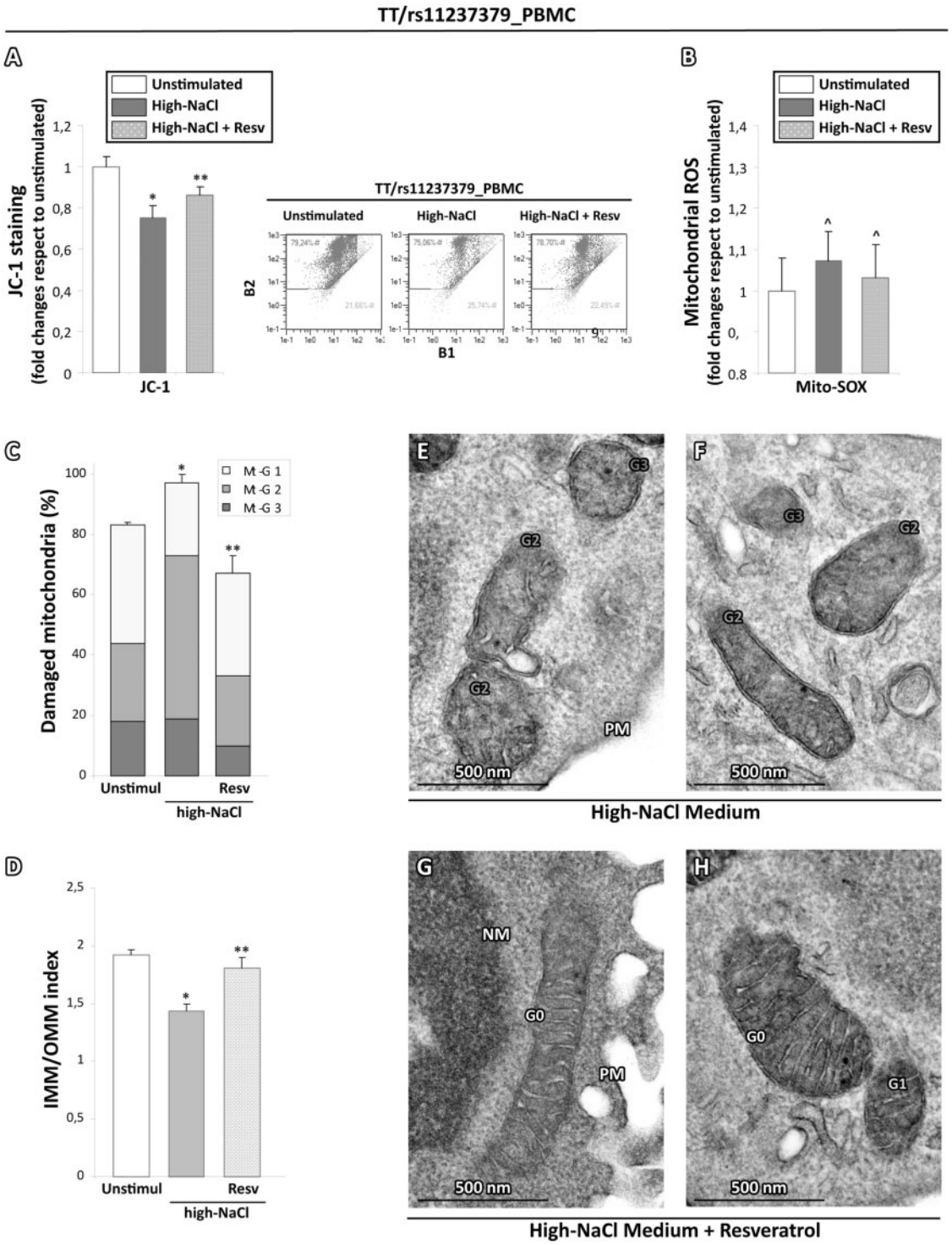

Figure 9. Effects of ROS scavenging on the high-salt dependent functional and ultrastructural impairment in mitochondria obtained from subjects with decreased NDUFC2 expression. (**A**) JC-1 cytofluorimetric assay for mitochondrial membrane potential evaluation. The pretreatment with resveratrol reduced the mitochondrial depolarization induced by salt stimulation (Student *t* test: $^{*}P < 0.05$ vs unstimulated PBMCs from TT carriers; $^{**}P < 0.05$ vs salt stimulated PBMCs from TT carriers). (**B**) Mito-SOX cytofluorimetric assay for mitochondrial ROS generation. The resveratrol tended to counteract the oxidative stress due to salt stimulation (Student T test: $^{\wedge}P$=NS versus unstimulated PBMCs from TT carriers). (C,**D**) Graphical representation of resveratrol effects on the ultrastructural damage due to salt stimulation in PBMCs from TT carriers. The overall damage (Mt-G1 + 2+3) and the loss of inner cristae (IMM/OMM index) were lower in PBMCs from TT carriers pretreated with resveratrol compared with salt stimulated PBMCs from TT carriers (Kruskal-Wallis test in (C and D): $^{**}P < 0.05$ vs untreated and salt stimulated PBMCs from TT carriers). **(E–H)** Representative micrographs of mitochondria in high-NaCl exposed PBMCs from TT carriers preatreated or not with resveratrol. After high-NaCl stimulus, the mitochondria PBMCs from TT carriers showed a noticeable loss of cristae (E and F); in contrast, PBMCs from TT carriers pretreated with resveratrol (G and H) displayed a recovery of ultrastructural integrity. (TEM micrographs, uranyl acetate/lead citrate; Legend: Nu, nucleus; NM, nuclear membrane, PM, plasma membrane; Gx: grade of mitochondrial damage).

convolution and IMM/OMM index. As expected, we have documented similar patterns of dysfunctional and ultrastructural alterations also in human PBMCs isolated from TT/rs11237379 carriers. As in other *in vitro* models of mitochondrial pathology (19), the high-salt medium, as well as the standardized proinflammatory stimulation with LPS, effectively unmasked the ultrastructural damage of mitochondria, highlighting a different adaptive capability of NDUFC2 deficient cells that may not be overt in basal conditions (20). Finally, the key role of increased oxidative stress on the mitochondrial impairment of NDUFC2 deficient cells has been confirmed by the counteracting effects of resveratrol, an antioxidant able to exert a strong inhibitory effect on intracellular and mitochondrial ROS generation.

The association of the major T allele of rs11237379 with decreased NDUFC2 expression, mitochondrial dysfunction, and increased risk of stroke in humans presents an obvious paradox if 44% of humans carry the TT/rs11237379 genotype. The T allele is also conserved across all primates. To investigate the potential functional consequences of genetic variation surrounding NDUFC2, we examined the Genotype-Tissue Expression (GTEx) project portal for evidence of expression differences associated to this haplotype. Importantly, GTEx confirms significant expression quantitative trait loci (eQTL) association in multiple tissues between a broad haplotype containing many linked SNPs centered around rs11237379 and *NDUFC2*, with the major T allele being associated with lower expression, as well as another local gene, *KCTD21* (see Supplementary Material, Fig. S2). Interestingly, KCTD21 is a Cullin3 adaptor protein which has been demonstrated as a negative regulator of Histone Deacetylase (HDAC1) (21). HDAC1 inhibition, in turn, has been demonstrated to improve recovery from ischemic white matter injury (22–24) an effect likely at least partially as a result of increased peroxisome proliferator-activated receptor gamma, coactivator 1 alpha (PGC1α) activity leading to increased mitochondrial biogenesis and oxygen consumption (25). Indeed, we confirmed that our TT and TC subjects, like NDUFC2, demonstrate markedly reduced KCT21 and PGC1a expression compared with CC/rs11237379 subjects (Supplementary Material, Fig. S2), suggesting a potential synergistic role between NDUFC2/Complex I dysfunction and dysregulation of PGC1α -mediated mitochondrial biogenesis. Future studies will be required to determine the actual functional variants in this haplotype which lead to altered expression of these genes and the relative contributions of their dysregulation.

In conclusion, both murine and human cell models used in our study share a close relationship between reduced expression of Ndufc2, mitochondrial dysfunction, altered oxidative metabolism and mitochondrial ultrastructural changes, particularly after the high-salt stimulus.

To our knowledge, we provide the first demonstration that Ndufc2 deficiency leads to a severe ultrastructural impairment of mitochondrial morphology also in human cells. Altogether, these findings provide additional insights on the key role of an altered pattern of mitochondrial structure–function as a cause of disease. Importantly, they underscore a possible novel genetic risk factor for human diseases that is frequently represented in the general population, a discovery which awaits confirmation by further larger studies. Notably, Ndufc2 can represent a new molecular target for therapeutic approaches aimed to combat the burden of cardiovascular diseases.

Materials and Methods

Establishment of fibroblast cultures from the *Ndufc2* knock-out rat model and treatments

Primary cultures of fibroblasts were obtained from skin samples (~1 cm^2) of a stroke-resistant spontaneously hypertensive rat (SHRSR) carrying the *Ndufc2* deletion in a heterozygous configuration (SHRSR_KO *Ndufc2*) (5). Control fibroblasts were obtained from skin of SHRSR wild-type rats (SHRSR_WT *Ndufc2*). Tissue samples were cut into small pieces, digested with dispase 0.1 mg/ml and collagenase I 0.35% for 45 min at 37 °C, pelleted, resuspended and maintained in Dulbecco's Modified Eagle Medium/Nutrient Mixture F-12 (DMEM/F-12, Sigma Chemicals Co., St Louis, MD, USA) containing 10% fetal bovine serum (FBS) and antibiotics. Primary cultures were propagated up to the third passage. For all experiments, cells were exposed or not to high-NaCl medium for 24–72 hours. High-NaCl medium was prepared by adding NaCl to standard medium DMEM/F-12 (120 mmol/l) to the final concentration of 145 mmol/l. For treatments with ROS scavenger, cells were pretreated with 3, 5, 4'-trihydroxy-trans-stilbene 50 μM (resveratrol; Sigma–Aldrich, St. Louis, MO, USA) left in the basal medium without serum for 12 hours before the exposure to high-NaCl medium.

Morphological and immunophenotypic analysis of fibroblast cultures from the *Ndufc2* knock-out rat model

For the fibroblast morphological analysis, the culture samples were observed on a Zeiss Axiovert 200 inverted microscope (Zeiss, Oberkochen, Germany) equipped with differential interference contrast (DIC) optics. Three differentiation stages were evaluated: FI = small spindle shaped cell, FII = small epithelioid cells, FIII = large epithelioid cells. The L: E differentiation index was calculated analysing the fibroblasts in early (E: FI, FII, FI/FII) and late (L: FII, FIII, FII/FIII) differentiation state (26). Quantitative analysis was performed by counting, for each cell culture, a total of at least 250 cells observed in five microscopic fields randomly taken from three different experiments.

For the immunophenotypic analysis, the culture samples were fixed with 4% paraformaldehyde followed by treatment with 0.1 M glycine for 20 min at 25 °C and with 0.1% Triton X-100 for additional 5 min at 25 °C to allow permeabilization. Cells were then incubated with the following primary antibodies: anti-vimentin (1: 50 in PBS; Dako, Glostrup, Denmark), anti-αSMA (1: 50 in PBS; Dako), and anti-cytokeratins FITC (1: 10 in PBS; Miltenyi Biotec, Bergish Gladbach, Germany) monoclonal antibodies. The unconjugated primary antibodies were visualized after appropriate washing with PBS by using goat anti-mouse IgG–FITC (1: 50 in PBS; Cappel Research Products, Durham, NC, USA) or goat anti-mouse Texas Red (1: 200 in PBS; Jackson Immunoresearch Laboratories, West Grove, PA, USA) for 30 min at 25 °C. Nuclei were stained with 4-6-diamido-2-phenylindole dihydrochloride (DAPI; 1: 10, 000 in PBS, Sigma Chemical Co., St. Louis, MO, USA). Coverslips were finally mounted with Mowiol in PBS for observation. Fluorescence signals were analysed by ApoTome System (Zeiss) connected with an Axiovert 200 inverted microscope (Zeiss).

Human PBMC cultures and treatments

Venous blood specimens were obtained after written informed consent from patients and volunteer healthy donors at time

designated in the protocol. The study was approved by the institutional review board of the Sapienza University of Rome (no. 1916/2015). Blood samples were taken from apparently healthy subjects ($n = 34$) homozygous for the minor allele (TT/rs11237379; $n = 9$), heterozygous (TC/rs11237379; $n = 16$), or homozygous for the major allele (CC/rs11237379; $n = 9$). Genotype assessment for the NDUFC2 variant was performed as previously reported (5). Samples were drawn into collection tubes containing EDTA, delivered directly to the Cellular Diagnostics Unit laboratory and immediately processed to isolate peripheral blood mononuclear cells (PBMCs) using density gradient centrifugation over Ficoll-Paque™ PLUS (Amersham Biosciences/GE Healthcare). PBMCs were cultured in duplicate at the density of 1×10^6 cells/ml on T25 flasks (Becton Dickinson, Oxnard, CA) in RPMI-1640 supplemented with 10% fetal bovine serum (FCS) and antibiotics and or not stimulated with 1 μg/ml Lipopolysaccharide S (LPS; Sigma Chemicals Co.) or with high-NaCl medium (RPMI-1640 at final concentration of 145 mmol/l) at 37 °C for times ranging from 3 to 48 h. For antioxidant treatment with ROS scavenger, PBMCs from subjects carrying the TT/rs11237379 ($n = 3$) and the CC/rs11237379 genotype ($n = 3$), were preloaded with 3, 5, 4'-trihydroxy-trans-stilbene 50 μM (resveratrol) left in the basal medium without serum for 12 hours before the exposure to high-NaCl medium. Cultured PBMCs were then divided into several aliquots that were used for flow cytometry and ultrastructural evaluation.

Assessment of mitochondrial membrane potential

For mitochondrial membrane potential ($\Delta\psi m$) assessment, the cells were incubated with CMXRosamine 100 nm (MT-Red™, Molecular Probes, Invitrogen) for 30 min at 37 °C, tetramethylrhodamine methyl ester (TMRM, Molecular Probes, Invitrogen) 500 nM for 30 min at 37 °C and with 5, 5′, 6, 6′-tetrachloro-1, 1′, 3, 3′-tetraethylbenzimidazolylcarbocyanine iodide 1.5 μM (JC-1, Molecular Probes) for 30 min at 37 °C. The samples were protected from light, washed with warmed PBS, resuspended in pre-warmed medium and collected with MACSQuantH Analyzer flow cytometer. The excitation and emission wavelengths were 488/585 nm (B2 channel) for TMRM analysis and 488/525 to 585 nm (B1 + B2 channels) for JC-1 polychromatic fluorescence emission evaluation. The fluorescence intensity of MT-Red™ (FIU, Fluorescence Intensity Units) was measured by Axiovision software (Zeiss) evaluating at least 300 cells for each condition in three different microscopic fields. To better visualize the differences of signal intensity, digital images were further analysed through a scale rainbow of pseudo-color (27). This function of the LSM 410 software (Zeiss) expresses the fluorescence intensity in a pseudo-color scale, in which white is the highest and brown-red is the lowest and shades of orange-yellow and green represent intermediate levels of intensity value in gray scale levels.

Reactive oxygen species detection

For ROS detection, the cells were incubated with 2', 7'-dichlorofluorescein diacetate (DCFH-DA, Sigma-Aldrich, St. Louis, MO, USA) 5 μM for 10 min at 37 °C for cytoplasmic oxidative stress assessment, or with MitoSOX™ Red mitochondrial superoxide indicator (Molecular Probes, Invitrogen, Eugene, OR) 1 μM for 15 min at 37 °C for mitochondrial oxidative stress assessment, protected from light, extensively washed with PBS, resuspended in pre-warmed medium and collected with MACSQuantH Analyzer flow cytometer (Miltenyi Biotec GmbH). The excitation and emission wavelengths were 488/525 nm (B1 channel) for DCFH-DA and 488/585 nm (B2 channel) for MitoSOX™ Red detection.

Analysis of cytofluorimetric signals

All fluorescence signals obtained from flow cytometer were analysed by MACSQuantify software (Miltenyi Biotec GmbH) and visualized on a three-decade log scale. For JC-1 analysis, the percentage of cells with a low mitochondrial membrane potential was obtained using a biparametric histogram with green versus red fluorescence and the mitochondrial depolarization index was indicated by a decrease of red to green fluorescence intensity ratio. The mean fluorescence intensity (MFI ± SE) of TMRM, DCFH-DA and Mito-SOX was calculated from three independent experiments with evaluation of at least 20 000 events for assay.

Transmission electron microscopy

Fibroblast cultures from rat model and human PBMCs treated as above, were washed three-times in PBS and fixed with 2% glutaraldehyde in PBS for 2 h at 4 °C. Samples were postfixed with 1% osmium tetroxide in veronal acetate buffer (pH 7.4) for 1 h at 25 °C, stained with uranyl acetate (5 mg/ml) for 1 h at 25 °C, dehydrated in acetone and embedded in Epon 812 (EMbed 812, Electron Microscopy Science, Hatfield, PA, USA). Ultrathin sections obtained with an Ultracut EMFCS ultramicrotome (Leica Microsystems, Wetzlar, Germany) were examined unstained or poststained with uranyl acetate and lead hydroxide under a Morgagni 268 D transmission electron microscope (FEI, Hillsboro, OR, USA) equipped with a Mega View II charge-coupled device camera (SIS, Soft Imaging System GmbH, Munster, Germany).

Ultrastructural quantitation of mitochondrial damage

At least 30 randomly taken cell sections in 10 different microscopic fields from ultrathin sections of each sample, were acquired at 28, 000X original magnification and digitalized with a Mega View II charge-coupled device camera (Soft Imaging System). The micrographs were analysed with the AnalySIS software (Soft Imaging System) for the percentage of damaged mitochondria classified using a grading scale based on the mitochondrial area with intact cristae, as previously described (10). Thus, injury grading was categorized into three levels of morphological mitochondria damage: Mt-G3, severe; Mt-G2, moderate and Mt-G1, slight, corresponding to 0, 1–50 and 51–75% of the area occupied by intact cristae. Also, an additional parameter of the mitochondrial injury was the convolution degeneration related to the inner mitochondrial membrane (IMM) length. All mitochondria observed in 20 ultrathin sections, randomly taken at 56, 000X for all samples, were measured for both lengths of IMM and Outer Mitochondrial Membrane (OMM); hence, the IMM/OMM index was calculated for each mitochondrion. Mitochondrial damage was correlated to a low mean value of IMM/OMM index, corresponding to partial or total loss of IMM cristae.

Statistical methods

Student's *t* test was used to evaluate statistical significance among variables that assume normal distribution. The values are expressed as mean ± SD from three independent experiments.

Kruskal-Wallis non-parametric test was used to compare variables that do not assume Gaussian distribution. The one-way ANOVA with test for linear trend was used to test the significance of variability values during time-course experiments. The one-way ANOVA with Dunnett's multiple comparison test was performed to compare all sets of experimental data to control set.

Supplementary Material

Supplementary Material is available at *HMG* online.

Acknowledgements

The data used for the analyses described in this manuscript were obtained from: the GTEx Portal on 06/20/17.

Conflict of Interest statement. None declared.

Funding

Italian Ministry of Health and from the 5‰ grant; Common Fund of the Office of the Director of the National Institutes of Health (The Genotype-Tissue Expression (GTEx) Project); NCI; NHGRI; NHLBI; NIDA; NIMH; NINDS. Funding to pay the Open Access publication charges for this article was provided by IRCCS Neuromed, Pozzilli, Italy.

References

1. Turrens, J.F. (2003) Mitochondrial formation of reactive oxygen species. *J. Physiol.*, **552**, 335–344.
2. Mimaki, M., Wang, M., McKenzie, M., Thorburn, D.R. and Ryan, M.T. (2012) Understanding mitochondrial complex I assembly in health and disease. *Biochim. Biophys. Acta*, **1817**, 851–862.
3. Rubattu, S., Stanzione, R. and Volpe, M. (2016) Mitochondrial dysfunction contributes to hypertensive target organ damage: lessons from an animal model of human disease. *Oxid. Med. Cell. Long.*, **2016**, 1067801.
4. Gershoni, M., Levin, L., Ovadia, O., Toiw, Y., Shani, N., Dadon, S., Barzilai, N., Bergman, A., Atzmon, G. and Wainstein, J. (2014) Disrupting mitochondrial-nuclear coevolution affects OXPHOS complex I integrity and impacts human health. *Genome Biol. Evol.*, **6**, 2665–2680.
5. Rubattu, S., Di Castro, S., Schulz, H., Geurts, A.M., Cotugno, M., Bianchi, F., Maatz, H., Hummel, O., Falak, S., Stanzione, R. *et al.* (2016) Ndufc2 gene inhibition is associated with mitochondrial dysfunction and increased stroke susceptibility in an animal model of complex human disease. *J. Am. Heart Assoc.*, **5**, pii: e002701.
6. Olsson, A.H., Rönn, T., Ladenvall, C., Parikh, H., Isomaa, B., Groop, L. and Ling, C. (2011) Two common genetic variants near nuclear-encoded OXPHOS genes are associated with insulin secretion in vivo. *Eur. J. Endocrinol.*, **164**, 765–771.
7. Igci, Y.Z., Bozgeyik, E., Borazan, E., Pala, E., Suner, A., Ulasli, M., Gurses, S.A., Yumrutas, O., Balik, A.A. and Igci, M. (2015) Expression profiling of SCN8A and NDUFC2 genes in colorectal carcinoma. *Exp. Oncol.*, **37**, 77–80.
8. Chin, S.F., Teschendorff, A.E., Marioni, J.C., Wang, Y., Barbosa-Morais, N.L., Thorne, N.P., Costa, J.L., Pinder, S.E., van de Wiel, M.A., Green, A.R. *et al.* (2007) High-resolution aCGH and expression profiling identifies a novel genomic subtype of ER negative breast cancer. *Genome Biol.*, **8**, R215.
9. Shi, J., Dai, W., Hale, S.I., Brown, D.A., Wang, M., Han, X. and Kloner, R.A. (2015) Bendavia restores mitochondrial energy metabolism gene expression and suppresses cardiac fibrosis in the border zone of the infarcted heart. *Life Sciences*, **141**, 170–178.
10. Putignani, L., Raffa, S., Pescosolido, R., Rizza, T., Del Chierico, F., Leone, L., Aimati, L., Signore, F., Carrozzo, R., Callea, F. *et al.* (2012) Preliminary evidences on mitochondrial injury and impaired oxidative metabolism in breast cancer. *Mitochondrion*, **12**, 363–369.
11. Leonard, S.S., Xia, C., Jiang, B.-H., Stinefelt, B., Klandorf, H., Harris, G.K. and Shi, X. (2003) Resveratrol scavenges reactive oxygen species and effects radical-induced cellular responses. *Biochem. Biophys. Res. Comm.*, **309**, 1017–1026.
12. 1000 Genomes Project Consortium, Auton, A., Brooks, L.D., Durbin, R.M., Garrison, E.P., Kang, H.M., Korbel, J.O., Marchini, J.L., McCarthy, S., McVean, G.A., Abecasis, G.R. *et al.* (2015) A global reference for human genetic variation. *Nature*, **526**, 68–74.
13. Hackenbrock, C.R. (1966) Ultrastructural bases for metabolically linked mechanical activity in mitochondria. I. Reversible ultrastructural changes with change in metabolic steady state in isolated liver mitochondria. *J. Cell. Biol.*, **30**, 269–297.
14. Hackenbrock, C.R. (1968) Ultrastructural bases for metabolically linked mechanical activity in mitochondria. II. Electron transport-linked ultrastructural transformations in mitochondria. *J. Cell. Biol.*, **37**, 345–369.
15. Scalettar, B.A., Abney, J.R. and Hackenbrock, C.R. (1991) Dynamics, structure, and function are coupled in the mitochondrial matrix. *Proc. Natl. Acad. Sci. USA*, **88**, 8057–8061.
16. Rossignol, R., Gilkerson, R., Aggeler, R., Yamagata, K., Remington, S.J. and Capaldi, A. (2004) Energy substrate modulates mitochondrial structure and oxidative capacity in cancer cells. *Cancer Res.*, **64**, 985–993.
17. Smeitink, J.A.M., van den Heuvel, L.W. and Di Mauro, S. (2001) The genetics and pathology of oxidative phosphorylation. *Nat. Rev. Genet.*, **2**, 342–352.
18. Willems, P.H.G.M., Smeitink, J.A.M. and Koopman, W.J.H. (2009) Mitochondrial dynamics in human NADH: ubiquinone oxidoreductase deficiency. *Int. J. Biochem. Cell. Biol.*, **41**, 1773–1782.
19. Carta, S., Tassi, S., Delfino, L., Omenetti, A., Raffa, S., Torrisi, M.R., Martini, A., Gattorno, M. and Rubartelli, A. (2012) Deficient production of IL-1 receptor antagonist and IL-6 coupled to oxidative stress in cryopyrin-associated periodic syndrome monocytes. *Ann. Rheum. Dis.*, **71**, 1577–1581.
20. Koopman, W.J., Distelmaier, F., Hink, M.A., Verkaart, S., Wijers, M., Fransen, J., Smeitink, J.A. and Willems, P.H. (2008) Inherited complex I deficiency is associated with faster protein diffusion in the matrix of moving mitochondria. *Am. J. Physiol. Cell. Physiol.*, **294**, C1124–C1132.
21. De Smaele, E., Di Marcotullio, L., Moretti, M., Pelloni, M., Occhione, M.A., Infante, P., Cucchi, D., Greco, A., Pietrosanti, L., Todorovic, J. *et al.* (2011) Identification and characterization of KCASH2 and KCASH3, 2 novel Cullin3 adaptors suppressing histone deacetylase and Hedgehog activity in medulloblastoma. *Neoplasia*, **13**, 374–385.
22. Baltan, S., Murphy, S.P., Danilov, C.A., Bachleda, A. and Morrison, R.S. (2011) Histone deacetylase inhibitors preserve white matter structure and function during ischemia by conserving ATP and reducing excitotoxicity. *J. Neurosci.*, **31**, 3990–3999.

23. Baltan, S., Morrison, R.S. and Murphy, S.P. (2013) Novel protective effects of histone deacetylase inhibition on stroke and white matter ischemic injury. *Neurotherapeutics*, **10**, 798–807.
24. Baltan, S., Bachleda, A., Morrison, R.S. and Murphy, S.P. (2011) Expression of histone deacetylases in cellular compartments of the mouse brain and the effects of ischemia. *Transl. Stroke. Res.*, **2**, 411–423.
25. Galmozzi, A., Mitro, N., Ferrari, A., Gers, E., Gilardi, F., Godio, C., Cermenati, G., Gualerzi, A., Donetti, E., Rotili, D. *et al.* (2013) Inhibition of class I histone deacetylases unveils a mitochondrial signature and enhances oxidative metabolism in skeletal muscle and adipose tissue. *Diabetes*, **62**, 732–742.
26. Raffa, S., Leone, L., Scrofani, C., Monini, S., Torrisi, M.R. and Barbara, M. (2012) Cholesteatoma-associated fibroblasts modulate epithelial growth and differentiation through KGF/FGF7 secretion. *Histochem. Cell. Biol.*, **138**, 251–269.
27. Leone, L., Mazzetta, F., Martinelli, D., Valente, S., Alimandi, M., Raffa, S. and Santino, I. (2016) Klebsiella pneumoniae Is Able to Trigger Epithelial-Mesenchymal Transition Process in Cultured Airway Epithelial Cells. *PLoS ONE*, **11**, e0146365.